SPE/DOE 35420

Development of Dual-Permeability Thermal Simulator and Validation for Yates Field

Philip H. Winterfeld, SPE, Marathon Oil Company

Abstract

Conservation equations for single-porosity and dual-permeability transport are similar except for matrix-fracture transport terms. A dual-permeability thermal simulator is developed starting from a single-porosity one by replicating the single-porosity grid, denoting one half of the grid to be fractures, the other half matrix, and introducing connections between analogous gridcells of the two halves that account for matrix-fracture transport. Consequences of replicating the single-porosity grid, which doubles the number of gridcells, are discussed. The dual-permeability simulator was developed to simulate steam injection in the Yates field. A two-dimensional and three-dimensional example of steam injection into a reservoir are shown. The two-dimensional example is used to validate the dual-permeability simulator by comparing results to a single-porosity simulation in which fractures are represented explicitly as narrow slits.

Introduction

Naturally fractured reservoirs are found throughout the world and contain significant amounts of oil reserves. They consist of a network of interconnected fractures surrounding porous matrix blocks. Most of the porosity of naturally fractured reservoirs is contained in the matrix. The fractures normally have little pore volume but are orders of magnitude more permeable than the matrix blocks. Recovery of oil from naturally fractured reservoirs is envisioned to take place in two steps: expulsion of oil from the matrix blocks followed by flow through the highly permeable fracture network to the well. Steam injection is a process used to recover oil from naturally fractured reservoirs. Several mechanisms operate during steam injection that force oil from matrix blocks into the fractures,[1] such as thermal expansion, capillary imbibition, gravity drainage, and distillation. Numerical simulation of steam injection into naturally fractured reservoirs requires a description of the geometry and properties of naturally fractured reservoirs plus a formulation of fluid and heat flow that can adequately handle the above recovery mechanisms.

Two idealized simulation models for naturally fractured reservoirs are dual-porosity and dual-permeability. In the dual-porosity model,[2-4] two types of porosity are found in a rock volume: fracture and matrix. Matrix porosity is entirely surrounded by fractures and the dual-porosity model has been visualized as a set of stacked sugar cubes, representing matrix blocks, separated by fractures. There is no communication between matrix blocks in the dual-porosity model but the fracture network is continuous. Matrix blocks do communicate with the fractures that surround it, however. The dual-permeability model[5,6] is similar to the dual-porosity model but allows communication between matrix blocks. Many examples of dual-porosity and dual-permeability numerical simulators have been reported.[7] Numerical simulators with the capability to simulate heat flow for dual-porosity reservoirs have been reported by Pruess et al.[8] and Chen et al.,[9] and those for dual-permeability reservoirs have been reported by Lee et al.[10] who simulated steam injection in a heavy oil reservoir and Oballa et al.[11] who used a multiphase and multicomponent formulation.

In this paper, a dual-permeability thermal simulator called THERMDK is developed. Starting with an existing single-porosity thermal simulator, THERM, modifications are introduced that transform the single-porosity simulator into a dual-permeability one. The dual-permeability simulator THERMDK was developed to simulate steam injection in the Yates field. The Yates field, located in West Texas, is a highly fractured reservoir with a large gas cap currently present.[12] Gravity drainage is the dominant

production drive mechanism and steam injection is being considered to facilitate oil recovery from the reservoir. Two simulations are shown as examples, a two-dimensional one and a three-dimensional one on an eighth of a ten-acre five-spot pattern. The two-dimensional example is also used as to validate THERMDK: a comparison is made to a single-porosity thermal simulator, CHEARS™ [13], in which fractures are explicitly represented as narrow slits.

Single-Porosity Thermal Simulator

THERM, the single-porosity thermal simulator, was developed by Coats.[14] It is a three-dimensional simulator. Fluid flow is governed by conservation of mass and Darcy's law and gravity, viscous, and capillary forces are included. Heat flow occurs by conduction and convection within the reservoir and there is conductive heat loss to the overburden and underburden. Reservoir fluid consists of four phases (water, oil, gas and solid) with any number of components that can be distributed in any of the phases by K-values that are functions of pressure and temperature. Phase density is a function of pressure, temperature, and composition and gas phase supercompressibility factor is obtained from the Redlich-Kwong equation of state.[15] Any number of chemical reactions may occur with each reaction having any number of reactants and products. Reaction rates are functions of temperature and reactant concentrations raised to the appropriate powers. The above formulation yields a set of mass and energy balance equations and constraints (fluid saturations sum to unity, component mole fractions in each phase sum to unity) that are solved using a fully implicit finite-difference approximation on a discretized reservoir.

Conservation Equations

Conservation equations for the single-porosity and dual-permeability models are shown in this section. Reservoir fluid is assumed to contain N_p phases and any number of components. The equations are written in finite-difference form because most numerical simulators are formulated that way. The dual-permeability model contains twice the number of equations as the single-porosity one because equations are written for both the fractures and matrix blocks.

Single-Porosity Model. For the single porosity model, conservation of mass for component "i" is

$$\Delta \sum_{p=1}^{N_p} T_r (\frac{k_r \xi x_i}{\mu})_p (\Delta p - \gamma \Delta D)_p$$
$$+ q_i + R_i - (\frac{V}{\Delta t}) \Delta_t (\phi \sum_{p=1}^{N_p} (x_i \xi S)_p) = 0. \tag{1}$$

The terms in Equation 1, in order of appearance, are due to convection, sources and sinks, chemical reactions, and mass accumulation. Conservation of energy is

$$\Delta \sum_{p=1}^{N_p} T_r (\frac{k_r \xi H}{\mu})_p (\Delta p - \gamma \Delta D)_p$$
$$+ \Delta (T_c \Delta T) + \Delta H_R$$
$$+ Q - (\frac{V}{\Delta t}) \Delta_t (\phi \sum_{p=1}^{N_p} (U \xi S)_p + \tag{2}$$
$$(1 - \phi) C_{PR} (T - T_i)) = 0.$$

The terms in Equation 2, in order of appearance, are due to convection, conduction, chemical reactions, sources and sinks, and energy accumulation.

Dual-Permeability Model. For the dual permeability model, conservation of mass for component "i" in the fractures is

$$\Delta \sum_{p=1}^{N_p} T_r (\frac{k_r \xi x_i}{\mu})_p (\Delta p - \gamma \Delta D)_p \Big]_f$$
$$+ q_i \Big]_f + R_i \Big]_f + \sum_{p=1}^{N_p} \sigma V (\frac{k_r \xi x_i}{\mu})_p (\Delta p - \gamma \Delta D)_p \Big]_{fm} - \tag{3}$$
$$(\frac{V}{\Delta t}) \Delta_t (\phi \sum_{p=1}^{N_p} (x_i \xi S)_p) \Big]_f = 0.$$

The terms in Equation 3 are similar to those in the single-porosity case, Equation 1, except for the fourth term which is due to fracture-matrix convection. Conservation of mass for component "i" in the matrix blocks is

$$\Delta \sum_{p=1}^{N_p} T_r(\frac{k_r \xi x_i}{\mu})_p (\Delta p - \gamma \Delta D)_p \Bigg]_m$$

$$+ q_i \Big]_m + R_i \Big]_m + \sum_{p=1}^{N_p} \sigma V(\frac{k_r \xi x_i}{\mu})_p (\Delta p - \gamma \Delta D)_p \Bigg]_{mf} - \quad (4)$$

$$(\frac{V}{\Delta t}) \Delta_t (\phi \sum_{p=1}^{N_p} (x_i \xi S)_p) \Bigg]_m = 0.$$

The terms in Equation 4 are the matrix analog of those in Equation 3. The fourth term, due to matrix-fracture convection, is the negative of that in Equation 3. Conservation of energy for the fractures is

$$\Delta \sum_{p=1}^{N_p} T_r(\frac{k_r \xi H}{\mu})_p (\Delta p - \gamma \Delta D)_p \Bigg]_f$$

$$+ \Delta(T_c \Delta T) \Big]_f + \Delta H_R \Big]_f + Q \Big]_f$$

$$+ \sum_{p=1}^{N_p} \sigma V(\frac{k_r \xi H}{\mu})_p (\Delta p - \gamma \Delta D)_p \Bigg]_{fm} + \quad (5)$$

$$\sigma_T V \Delta T \Big]_{fm} -$$

$$(\frac{V}{\Delta t}) \Delta_t (\phi \sum_{p=1}^{N_p} (U \xi S)_p + (1 - \phi) C_{PR}(T - T_i)) \Bigg]_f = 0.$$

The terms in Equation 5 are similar to the single-porosity case, Equation 2, except for the fifth term, which is due to fracture-matrix convection, and the sixth term, which is due to fracture-matrix conduction. Conservation of energy for the matrix blocks is

$$\Delta \sum_{p=1}^{N_p} T_r(\frac{k_r \xi H}{\mu})_p (\Delta p - \gamma \Delta D)_p \Bigg]_m$$

$$+ \Delta(T_c \Delta T) \Big]_m + \Delta H_R \Big]_m$$

$$+ Q \Big]_m + \sum_{p=1}^{N_p} \sigma V(\frac{k_r \xi H}{\mu})_p (\Delta p - \gamma \Delta D)_p \Bigg]_{mf} + \quad (6)$$

$$\sigma_T V \Delta T \Big]_{mf} -$$

$$(\frac{V}{\Delta t}) \Delta_t (\phi \sum_{p=1}^{N_p} (U \xi S)_p + (1 - \phi) C_{PR}(T - T_i)) \Bigg]_m = 0.$$

The terms in Equation 6 are the matrix analog of those in Equation 5. The fifth term, due to matrix-fracture convection, and the sixth term, due to matrix-fracture conduction, are the negative of those in Equation 5. The single-porosity and dual-permeability equations are very similar. The same terms appear in both except for the fracture-matrix transport terms (subscripted "mf" or "fm") in the dual-permeability equations.

Dual-Permeability Modifications

The similarity between the single-porosity and dual-permeability conservation equations facilitates the modification of the single-porosity thermal simulator to a dual-permeability one. The conservation equations are solved on a reservoir discretized into gridcells. In a single-porosity reservoir, porosity is uniform in a gridcell and adjacent gridcells are connected, as shown in Figure 1. In a dual-permeability system, each gridcell contains fractures and matrix blocks. Although in reality fractures and matrix blocks are of irregular size and irregularly distributed in a gridcell, each gridcell will be portrayed here as containing a large number of matrix blocks of uniform size, the fracture spacings, separated by fractures. In addition, because properties in a gridcell are uniform, the matrix blocks are grouped in the center of the gridcell forming one large matrix block and the fractures are grouped surrounding the matrix block. Figure 2 shows a dual-permeability grid. As in the single-porosity case, adjacent gridcells are connected. However, this connection is between both the matrix blocks and the fractures of adjacent gridcells. Also, within each gridcell, there is a connection between the matrix block and the fractures. An alternate representation of the dual-permeability grid is shown in Figure 3. Matrix blocks are "lifted" out of the grid forming a second grid adjacent to the original. The original grid contains fracture porosity and the connections between fractures of adjacent gridcells. The second grid contains matrix porosity and the connections between matrix blocks of adjacent gridcells. The connections between analogous gridcells of the two grids represent fracture-matrix connections. Comparing Figure 3 to Figure 1, the connectivity of a single-porosity grid is transformed into that of a dual-permeability grid by replicating the grid (doubling the number of gridcells in one direction), adding connections between analogous gridcells of the two grid halves, and removing the connections between the two grid halves. Because the conservation equations are gravity dependent, a direction orthogonal to the gravity vector, the x-direction, is used to replicate the grid. The left half of the grid contains fracture porosity and the right half, matrix porosity. Except for matrix-fracture transport, the conservation equations for matrix and fracture have the same form as the single-porosity ones

and hence can be simulated using the existing single-porosity code. Connections between grid halves are removed by setting fluid and thermal transmissibilities there to zero. Fracture-matrix transport has a formulation similar to single-porosity flow between adjacent gridcells with the shape factor given by[16,17]

$$\sigma = 4 \left(\frac{k_x}{L_x^2} + \frac{k_y}{L_y^2} + \frac{k_z}{L_z^2} \right) \Bigg|_m . \qquad (7)$$

The shape factor for heat conduction is

$$\sigma_T = 4 \left(\frac{k_{Tx}}{L_x^2} + \frac{k_{Ty}}{L_y^2} + \frac{k_{Tz}}{L_z^2} \right) \Bigg|_m . \qquad (8)$$

Fracture-matrix transport is conveniently added to the code where calculation of transport between connected gridcells is done. Instead of using adjacent gridcells, pairs of analogous gridcells of the two grid halves are used, and the transmissibility between them is σV for fluid flow and $\sigma_T V$ for heat flow.

The dual-permeability model reduces to the dual-porosity model when there is no communication between matrix gridcells. Thus, by setting thermal and fluid transmissibilities to zero in the matrix portion of the grid, a dual-porosity simulation is obtained.

The grid replication that transforms the single-porosity grid to dual-permeability doubles the number of gridcells. Assigning the correct fracture and matrix porosities to the apppropriate grid halves will account for total fluid volume accurately. However, the total rock volume will be excessive. The actual rock volume is

$$(V_R)_a = V(1 - \phi_f - \phi_m). \qquad (9)$$

But, the rock volume in the simulation is

$$(V_R)_s = V[(1 - \phi_f) + (1 - \phi_m)]. \qquad (10)$$

This difference between actual rock volume and rock volume in the simulation would result in excess rock thermal capacity if it were not remedied by choosing matrix and fracture rock heat capacity such that rock thermal capacity in the simulation is equal to the actual value

$$C_{PR}(1 - \phi_f - \phi_m) = C_{Pf}(1 - \phi_f) + C_{Pm}(1 - \phi_m). \qquad (11)$$

Another relation is needed to uniquely determine matrix and fracture rock heat capacity: if rock is associated mostly with matrix, fracture heat capacity can be just a few percent of matrix heat capacity. Doubling the number of gridcells also doubles the area for heat loss to the overburden and underburden. The single-porosity simulator has an area multiplier that can correct for this area doubling. If rock is associated mostly with matrix, the matrix area multiplier can be set close to one and the fracture area multiplier close to zero to get the correct area.

The effective permeability of a fractured reservoir is given by

$$k_e = k_m + k_f \phi_f \qquad (12)$$

The permeability of the porous rock without the fractures, k_m, is used to calculated matrix-matrix transmissibilities and the effective fracture permeability, $k_f \phi_f$, is used to calculate fracture-fracture transmissibilities.

A well is situated in a z-direction column of gridcells. Thus, a well resides entirely in the fracture portion of the grid or the matrix portion, but not both. In reality, a well interacts with both fractures and matrix. A remedy for this is to specify two wells, one in the fracture gridcells and the other in the analogous matrix gridcells, and allocate well constraints based on the ratio of permeabilities there. In cases where fracture permeability is much greater than matrix permeability, omitting the well in the matrix gridcells can have little effect on a simulation.

Two-Dimensional Example

The two-dimensional example is a cross section (x-z) with two wells, a steam injector at one end and a producer at the other. The reservoir description is shown in Table 1. Reservoir fluid is three-phase, water-oil-gas and there is one water component and two hydrocarbon ones, OIL and GAS. Hydrocarbon component properties are shown in Table 2. The reservoir is initialized with oil phase and mostly residual water phase in both the fractures and matrix blocks. Oil phase initially has a uniform composition of 0.838 OIL and 0.162 GAS. Distribution of hydrocarbon components in the oil and gas phases is governed by K-values calculated[14] from the parameters shown in Table 3. The oil phase is the master phase for both hydrocarbon components. Oil and gas phase viscosities are calculated[14] from parameters shown in Tables 4 and 5, respectively. Water-oil and gas-oil relative permeability and capillary pressure data for the matrix are shown in Tables 6 and 7. For the fractures, capillary pressure is zero and phase relative permeability equals phase saturation. The steam injector, located at I=1, is completed in K=2-4 and the producer, located at I=5, is completed in K=8-9. The productivity indices of the producer and

injector layers are, respectively, 2 and 2.5 in field units. Three bbl/d of fluid at reservoir conditions are produced and 0.80 quality steam at 475°F at a bottomhole pressure of 475 psi is injected for five years.

Figure 4 shows temperature in the fractures at five years. The temperature at the injector is the highest and heat has traveled through the reservoir to the producer, elevating the temperature there over the initial uniform value of 82°F. Matrix temperature is slightly less than fracture temperature; the matrix-fracture thermal transmissibility is high but the matrix has a larger thermal capacity than the fractures because most of the reservoir rock is associated with the matrix. Figures 5a and 5b show oil saturation in the matrix and fractures, respectively, then. Much oil has been recovered from K=1-4 of the matrix and only a band of oil saturation is present in the fractures in K=6-9. Below the oil saturation band is water that fell there as injected steam gave up its heat to rock and condensed; above the band is gas composed of mostly water component from injected steam in I=1,2 and mostly GAS component liberated from hydrocarbon in I=3-5. OIL component is also present in the gas phase in small amounts. About 27.4 percent of the oil originally in place has been recovered. Figure 6 shows oil production rate versus time. Oil production rate levels out after about 200 days to about 0.6 bbl/d. The steam/oil ratio is shown in Figure 7. Between 3 and 4 bbl water equivalent of steam is required to produce 1 bbl of oil for most of the simulation.

The two-dimensional example was used to validate THERMDK by comparing its results to CHEARS, a single-porosity thermal simulator, that represented fractures as narrow slits. The two simulators produced slightly different steam injection schedules for the same well constraints. The steam/oil ratio after five years of steam injection versus cumulative water injected was compared. Two cases were run for each simulator and the results are shown in Figure 8. The trend lines coincide, indicating that the simulators agree on the amount of oil recovered per barrel of steam injected.

Three-Dimensional Example

The three-dimensional example is on an eighth of a ten-acre, five-spot pattern with an initial gas cap. The reservoir description of the three-dimensional example appears in Table 8. Figure 9 shows a cross section (x-y) of the grid with the reservoir boundary superimposed. Pore volume, rock heat capacity and z-direction face area, among others, are multiplied by the factors shown in the figure to account for the triangular geometry of the pattern. These factors apply to both fracture and matrix gridcells. Reservoir fluid and PVT properties are the same as the two-dimensional example and appeared in Tables 2-5. Relative permeability and capillary pressure for the matrix are shown in Tables 9 and 10 and for the fractures, Tables 11

and 12. Fracture relative permeability has been smoothed around saturations of zero and one. There are two wells, a steam injector located at I=1, J=1 and completed in K=1-3, and a producer located I=1, J=5 and completed in K=8-9. The productivity indices of the producer and injector layers are, respectively, 2.5 and 250. Thirty bbl/d of fluid at reservoir conditions is produced with a maximum gas production rate of 15 mcf/d and 0.80 quality steam at 450°F at a bottomhole pressure of 495 psi is injected for seven years.

Temperature in the vertical plane containing both wells is shown in Figures 10a and 10b. In Figure 10a, at 3-1/2 years, the temperature surface is fully developed in the column containing the injector, but falls off as you move toward the producer. In Figure 10b, at 7 years, the surface is fully developed. Matrix oil saturation is shown in Figures 11a-c. Figure 11a shows initial oil saturation with an oil zone located between the gas cap and a water leg. In Figure 11b, at 3-1/2 years, the surface edge around the injector has drifted down as injected steam displaces oil. The middle hump has slumped significantly as well. In Figure 11c, at 7 years, there is a large region around the injector devoid of oil and the slump of the middle hump has intensified. At this point 51.1% of the oil originally in place has been recovered. Figure 12 shows oil production rate versus time. Production peaks around 1800 days and starts to decline past 2000 days. Figure 13 shows steam-oil ratio versus time. This ratio is in the 4 to 8 range through most of the simulation, with a minimum corresponding to the maximum oil production rate around 1800 days, and the ratio increases as production declines after 2000 days.

Conclusions

1. A dual-permeability thermal simulator, THERMDK, was developed using a single-porosity thermal simulator, THERM, as the starting point.

2. The methodology used to develop the dual-permeability simulator is based on the form of the conservation equations governing transport and the finite-difference grid used to solve these equations. These equations and grid are common to many other simulators; hence, this methodology can be applied to them also.

3. The dual-permeability simulator was validated by comparison to a single-porosity simulator where fractures were represented as narrow slits.

4. The dual-permeability simulator simulated steam injection in a two- and three-dimensional reservoir adequately and will be used to do the same for the Yates field.

Nomenclature

C_p	=	heat capacity, L^2/t^2-deg, Btu/lbm-°F
C_{PR}	=	rock heat capacity, m/Lt^2-deg, Btu/ft^3-°F
D	=	depth, L, ft
H	=	enthalpy, mL^2/t^2, Btu
I	=	x-direction gridcell index
J	=	y-direction gridcell index
k	=	permeability, L^2, md
k_r	=	relative permeability
k_T	=	thermal conductivity, mL/t^3-deg, Btu/d-ft-°F
K	=	z-direction gridcell index
L	=	fracture spacing, L, ft
p	=	pressure, mL/t^2, psi
q	=	component source or sink, m/t, moles/d
Q	=	heat source or sink, mL^2/t^3, Btu/d
R	=	reaction rate, m/t, moles/d
S	=	phase saturation
t	=	time, t, d
T	=	temperature, °F
T_c	=	thermal transmissibility, mL^2/t^3-deg, Btu/d-°F
T_i	=	reference temperature, °F
T_r	=	transmissibility, L^3, bbl-cp/d-psi
U	=	internal energy, mL^2/t^2, Btu
V	=	gridcell volume, L^3, ft^3
V_R	=	rock volume, L^3, ft^3
x	=	mole fraction
γ	=	gradient, m/t^2, psi/ft
Δ	=	difference operator
Δ_t	=	time difference operator
ΔH_R	=	heat of reaction, mL^2/t^3, Btu/d
μ	=	viscosity, m/Lt, cp
ξ	=	molar density, m/L^3, moles/ft^3
σ	=	shape factor, md/L^2
σ_T	=	thermal shape factor, m/Lt^3-deg, Btu/d-ft^3-°F
ϕ	=	porosity

Subscripts

a	=	actual
e	=	effective
f	=	fracture
fm	=	fracture-matrix
g	=	gas phase
i	=	component
m	=	matrix
mf	=	matrix-fracture
o	=	oil phase
p	=	phase
R	=	rock
s	=	simulation
w	=	water phase
x	=	x-direction
y	=	y-direction
z	=	z-direction

References

1. Reis, J.C.: "Oil Recovery Mechanisms in Fractured Reservoirs During Steam Injection," paper SPE 20204 presented at SPE/DOE Seventh Symposium on Enhanced Oil Recovery, Tulsa, OK, April 22-24, 1990.

2. Warren, J.E. and Root, P.J.: "The Behavior of Naturally Fractured Reservoirs," Soc. Pet. Eng. J. (Sept. 1963) 245.

3. Kazemi, H.: "Pressure Transient Analysis of Naturally Fractured Reservoirs With Uniform Fracture Distribution," Soc. Pet. Eng. J. (Dec. 1969) 451.

4. Reis, J.C.: The Reservoir Engineering Aspects of Fractured Formations, Gulf Publishing Co., 1980.

5. Barenblatt, G.I., Zheltov, Iu.P., and Kochina, I.N.: "Basic Concepts in the Theory of Seepage of Homogeneous Liquids in Fissured Rocks," PMM, Vol. 24, No. 5, 1960.

6. Hill A.C. And Thomas G.W.: "A New Approach for Simulating Complex Reservoirs," paper SPE 13537 presented at SPE Reservoir Simulation Symposium, Dallas, Feb. 10-13, 1985.

7. Kazemi, H. and Gilman, J.R.: Flow and Contaminant Transport in Fissured Rock, chapter 6, Academic Press, 1993.

8. Pruess, K. And Narasimhan, T.N.: "A Practical Method for Simulating Fluid and Heat Flow in Fractured Porous Media," Soc. Pet. Eng. J. (Feb. 1985) 15.

9. Chen, W.H., Wasserman, M.L., and Fitzmorris, R.E.: "A Thermal Simulator for Naturally Fractured Reservoirs," paper SPE 16008 presented at Ninth SPE Symposium on Reservoir Simulation, San Antonio, TX, Feb. 1-4, 1987.

10. Lee, B.Y.Q. and Tan, T.B.S.: "Application of a Multiple Porosity/Permeability Simulator in Fractured Reservoir Simulation, paper SPE 16009 presented at Ninth SPE Symposium on Reservoir Simulation, San Antonio, TX, Feb. 1-4, 1987.

11. Oballa, V., Coombe, D.A. And Buchanan, W.L.: "Factors Affecting the Thermal Response of Naturally Fractured Reservoirs," paper CIM/AOSTRA 91-53 presented at CIM/AOSTRA Technical Conference, Banff, April 21-24, 1991.

12. Gilman, J.R., Bowzer, J.L., and Rothkopf, B.W.: "Application of Short-Radius Horizontal Boreholes in the Naturally Fractured Yates Field," paper SPE 28586 presented at SPE 69th Annual Technical Conference and Exhibition, New Orleans, LA, Sept. 25-28, 1994.

13. Chien, M.C.H., Yardumian, H.E., Chung, E.Y., and Todd, W. W.: "The Formulation of a Thermal Simulation Model in a Vectorized, General Purpose Reservoir Simulator," paper SPE 18418 presented at SPE Symposium on Reservoir Simulation, Houston, TX, Feb. 6-8, 1989.

14. Coats, K.H.: "In-Situ Combustion Model," Soc. Pet. Eng. J., (Dec. 1980) 533.

15. Redlich, O. and Kwong, J.N.S.: "On the Thermodynamics of Solutions. V. An Equation of State. Fugacities of Gaseous Solutions," Chem. Rev. (Feb. 1949) 233.

16. Kazemi, H., Merrill, L.S., Jr., Porterfield, K.L., and Zeman, P.R.: "Numerical Simulation of Water-Oil Flow in Naturally Fractured Reservoirs," Soc. Pet. Eng. J. (Dec. 1976) 317.

17. Rossen, R.H. and Shen, E.I.: "Simulation of Gas/Oil Drainage and Water/Oil Imbibition in Naturally Fractured Reservoirs," paper SPE 16982 presented at SPE 62nd Annual Technical Conference and Exhibition, Dallas, TX, Sept. 27-30, 1987.

SI Metric Conversion Factors

bbl × 1.589 873	E-01 = m^3
Btu × 1.055 056	E-00 = kJ
cp × 1.0*	E-03 = Pa•s
ft × 3.048*	E-01 = m
(°F+459.67)/1.8	= K
lbm × 4.535 924	E-01 = kg
psi × 6.894 75	E+00 = kPa
°R/1.8	= K

*Conversion factor is exact.

TABLE 1 - TWO-DIMENSIONAL RESERVOIR DESCRIPTION

Grid (2*NX, NY, NZ)	=	10, 1, 10.
x-direction thickness	=	10 ft.
y-direction thickness	=	5 ft.
z-direction thickness	=	30, 8*10, 30 ft.
Fracture spacing (x,y,z)	=	10, 10, 0 ft.
Depth to top of reservoir	=	-1255 ft.
Location of water-oil contact	=	-1100 ft.
Pressure at water-oil contact	=	460 psi.
Porosity	=	0.01 (fracture), 0.18 (matrix).
Matrix permeability (x,y,z)	=	100, 100, 30 md.
Effective fracture permeability (x,y,z)	=	100, 100, 100 md.
Rock heat capacity	=	35 Btu/ft³-°F.
Rock thermal conductivity	=	48 Btu/ft d-°F.
Over-/underburden heat capacity	=	35 Btu/ft³-°F.
Over-/underburden thermal conductivity	=	48 Btu/ft -d-°F.

TABLE 2 - HYDROCARBON COMPONENT PROPERTIES

Property	OIL	GAS
Molecular weight, lbm/mole	235.	30.
Critical pressure, psi	335.	3250.
Critical temperature, °R	1500.	545.
Compressibility, 1/psi	4.5e-6	9.0e-6
Thermal expansion coef., 1/°F	4.5e-4	8.0e-4
Heat capacity, Btu/lbm-°F	0.493	0.610
Stocktank density, lbm/ft³	55.0	30.0

TABLE 3 - HYDROCARBON K-VALUES

Component	KV1	KV2, psi	KV3,1/psi	KV4, °R	KV4, °R
OIL	10.	4000.	1.0E-3	7085.1	-298.53
GAS	-1.	7098.	3.62E-5	396.38	80.0

TABLE 4 - OIL PHASE VISCOSITY

Temperature, °F	μ_{oil}	μ_{gas}
80	14.8	0.376
100	10.5	0.352
120	7.58	0.332
160	4.22	0.296
200	2.52	0.266
260	1.29	0.230
320	0.73	0.202
380	0.446	0.179
400	0.367	0.160
500	0.317	0.150

TABLE 5 - GAS PHASE VISCOSITY

Temperature, °F	μ_{oil}	μ_{gas}
700	0.013	0.012
1000	0.015	0.014

TABLE 6 - WATER-OIL RELATIVE PERMEABILITY AND CAPILLARY PRESSURE

S_w	k_{rw}	k_{row}	P_{cwo}
0.0500	0.0000	1.0000	2.2
0.0700	0.0070	0.8900	0.68
0.1042	0.0100	0.6298	-0.28
0.1384	0.0152	0.4299	-0.63
0.1726	0.0250	0.2934	-0.78
0.2068	0.0499	0.2003	-0.85
0.2410	0.0700	0.1367	-0.89
0.2752	0.0857	0.0933	-0.90
0.3094	0.1020	0.0637	-0.92
0.3436	0.1212	0.0435	-0.95
0.3778	0.1400	0.0297	-0.98
0.4804	0.1892	0.0094	-1.00
0.5830	0.2400	0.0030	-1.02
0.6856	0.2900	0.0003	-1.10
0.7540	0.3164	0.0000	-1.20
0.8000	0.8000	0.0000	-1.40
0.8750	0.8500	0.0000	-2.00
0.9500	0.8800	0.0000	-4.00
1.0000	0.9000	0.0000	-11.68

TABLE 7 - OIL-GAS RELATIVE PERMEABILITY AND CAPILLARY PRESSURE

S_l	k_{rog}	k_{rg}	P_{cgo}
0.2960	0.0000	0.7500	4.5
0.3644	0.0009	0.7131	3.20
0.4670	0.0030	0.6105	2.30
0.5696	0.0094	0.4705	1.70
0.6722	0.0297	0.3168	1.15
0.7064	0.0435	0.2666	1.00
0.7406	0.0637	0.2184	0.90
0.7748	0.0933	0.1730	0.76
0.8090	0.1367	0.1313	0.64
0.8432	0.2003	0.0942	0.50
0.8774	0.2934	0.0626	0.40
0.9116	0.4299	0.0374	0.30
0.9458	0.6298	0.0194	0.19
0.9800	0.8900	0.0000	0.07
1.0000	1.0000	0.0000	0.00

TABLE 8 - THREE-DIMENSIONAL RESERVOIR DESCRIPTION

Grid (2*NX, NY, NZ)	=	10, 3, 14.
x-direction thickness	=	113 ft.
y-direction thickness	=	113 ft.
z-direction thickness	=	3*30, 9*10, 20, 100 ft.
Fracture spacing (x,y,z)	=	10, 10, 0 ft.
Depth to top of reservoir	=	-1390 ft.
Porosity	=	0.01 (fracture), 0.20 (matrix).
Matrix permeability (x,y,z)	=	100, 100, 72 md.
Effective fracture permeability (x,y,z)	=	5000, 5000, 5000 md.
Rock heat capacity	=	35 Btu/ft³-°F.
Rock thermal conductivity	=	48 Btu/ft -d-°F.
Over-/underburden heat capacity	=	35 Btu/ft³-°F.
Over-/underburden thermal conductivity	=	48 Btu/ft -d-°F.
Initial layer pressure	=	475., 475.3, 475.6, 479.6, 482.6, 485.6, 488.6, 491.6, 495.1, 499.4, 503.7, 511., 536.8 psi.
Initial layer water saturation	=	9*0.01, 4*0.95, 1.0 (fracture), 9*0.11, 4*0.90,1.0 (matrix).
Initial layer oil saturation	=	3*0.0, 0.10, 5*0.90, 4*0.05, 1.0 (fracture), 0.485, 0.525, 0.550, 0.720,5*0.890, 4*0.10, 0.0 (matrix).

223

TABLE 9 - MATRIX WATER-OIL RELATIVE PERMEABILITY AND CAPILLARY PRESSURE

S_w	k_{rw}	k_{row}	P_{cwo}
0.110	0.0	0.89000	2.2
0.152	0.0	0.53288	-0.28
0.194	0.0	0.31032	-0.63
0.236	0.0	0.17522	-0.85
0.278	0.00016	0.09566	-0.90
0.320	0.00049	0.05012	-0.92
0.362	0.00122	0.02514	-0.94
0.404	0.00263	0.01198	-0.95
0.446	0.00512	0.00538	-0.96
0.488	0.00923	0.00225	-0.98
0.530	0.01563	0.00087	-1.00
0.572	0.02516	0.00030	-1.02
0.614	0.03888	0.00009	-1.04
0.656	0.05801	0.00007	-1.06
0.698	0.08403	0.00006	-1.08
0.740	0.11865	0.00005	-1.10
0.824	0.22185	0.00002	-1.25
0.866	0.29524	0.00001	-1.40
0.900	0.38689	0.0	-2.00
1.000	0.50000	0.0	-11.0

TABLE 10 - MATRIX OIL-GAS RELATIVE PERMEABILITY AND CAPILLARY PRESSURE

S_l	k_{rog}	k_{rg}	P_{cgo}
0.210	0.0	0.78223	7.531
0.290	0.00008	0.73171	4.638
0.310	0.00013	0.71304	4.168
0.356	0.00026	0.66259	3.349
0.3872	0.00040	0.62325	2.949
0.4184	0.00060	0.58055	2.637
0.4808	0.00130	0.48775	2.178
0.5120	0.00190	0.43899	1.995
0.5432	0.00275	0.38954	1.828
0.5744	0.00430	0.34008	1.669
0.6368	0.00932	0.24380	1.360
0.6680	0.01365	0.19831	1.209
0.7304	0.02930	0.11598	0.922
0.7616	0.04923	0.08049	0.791
0.7928	0.06290	0.04966	0.671
0.8240	0.09215	0.02417	0.563
0.8864	0.19781	0.0	0.377
0.9488	0.42461	0.0	0.195
0.9800	0.60000	0.0	0.078
1.0000	0.89000	0.0	0.0

TABLE 11 - FRACTURE WATER-OIL RELATIVE PERMEABILITY AND CAPILLARY PRESSURE

S_w	k_{rw}	k_{row}	P_{cwo}
0.01	0.0	1.0	0.0
0.015	0.0005	0.9995	0.0
0.02	0.002	0.998	0.0
0.03	0.005	0.995	0.0
0.04	0.010	0.990	0.0
0.05	0.020	0.980	0.0
0.06	0.0302	0.9698	0.0
0.08	0.0507	0.949	0.0
0.09	0.061	0.939	0.0
0.10	0.070	0.930	0.0
0.91	0.930	0.070	0.0
0.92	0.939	0.061	0.0
0.93	0.9493	0.0507	0.0
0.95	0.9698	0.0302	0.0
0.96	0.980	0.020	0.0
0.97	0.990	0.010	0.0
0.98	0.995	0.005	0.0
0.99	0.998	0.002	0.0
0.995	0.9995	0.0005	0.0
1.00	1.0	0.0	0.0

TABLE 12 - FRACTURE OIL-GAS RELATIVE PERMEABILITY AND CAPILLARY PRESSURE

| S_l	k_{rog}	k_{rg}	P_{cgo}
0.01	0.0	1.0	1.000
0.015	0.0005	0.9995	0.999
0.02	0.002	0.998	0.996
0.03	0.005	0.995	0.990
0.04	0.010	0.990	0.980
0.05	0.020	0.980	0.960
0.06	0.0302	0.9698	0.9396
0.08	0.0507	0.9493	0.8986
0.09	0.061	0.939	0.8780
0.10	0.070	0.930	0.8600
0.91	0.93	0.070	-0.8600
0.92	0.939	0.061	-0.8780
0.93	0.9493	0.0507	-0.8986
0.95	0.9698	0.0302	-0.9396
0.96	0.980	0.020	-0.960
0.97	0.990	0.010	-0.980
0.98	0.995	0.005	-0.990
0.99	0.998	0.002	-0.996
0.995	0.9995	0.0005	-0.999
1.00	1.0	0.0	-1.0
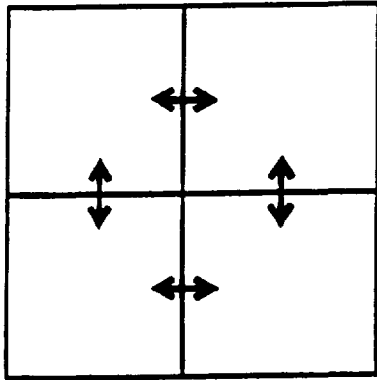
Figure 1.

Single-porosity grid. Arrows denote connections between gridcells.
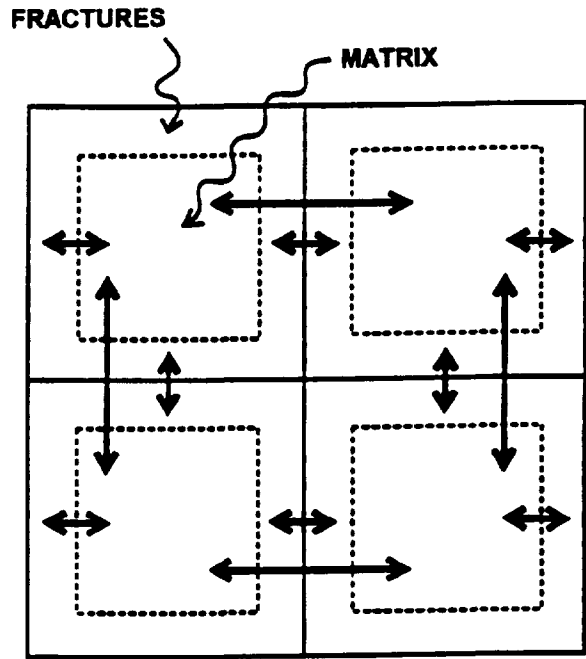

FIGURE 2

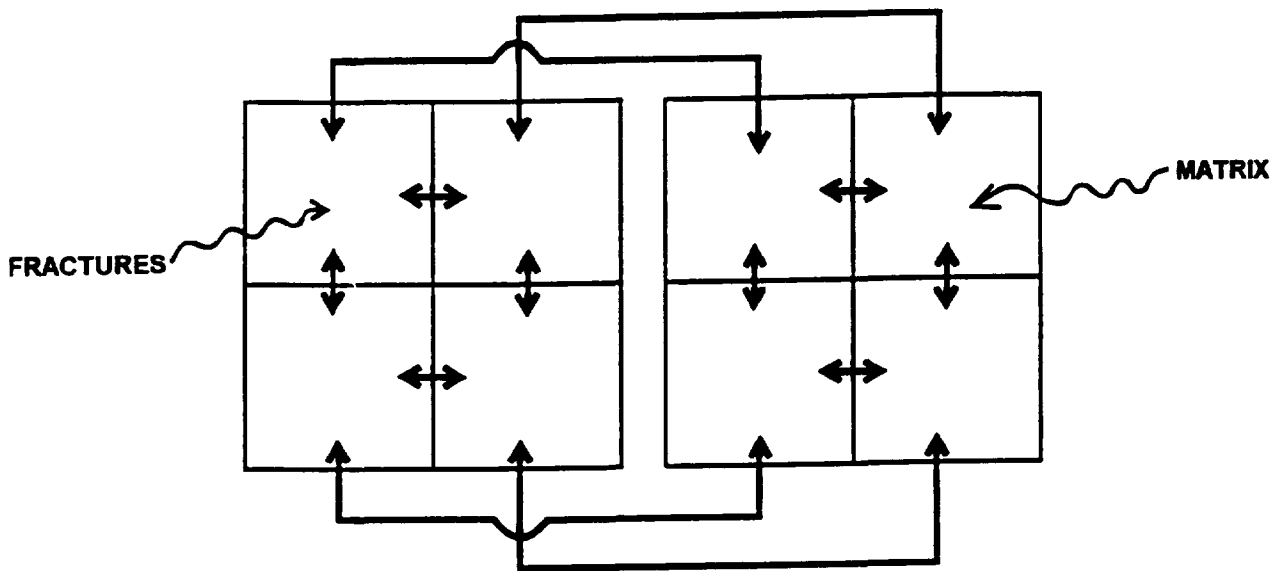Dual-permeability grid. Arrows denote connections between matrix and fractures in gridcells.

FIGURE 3

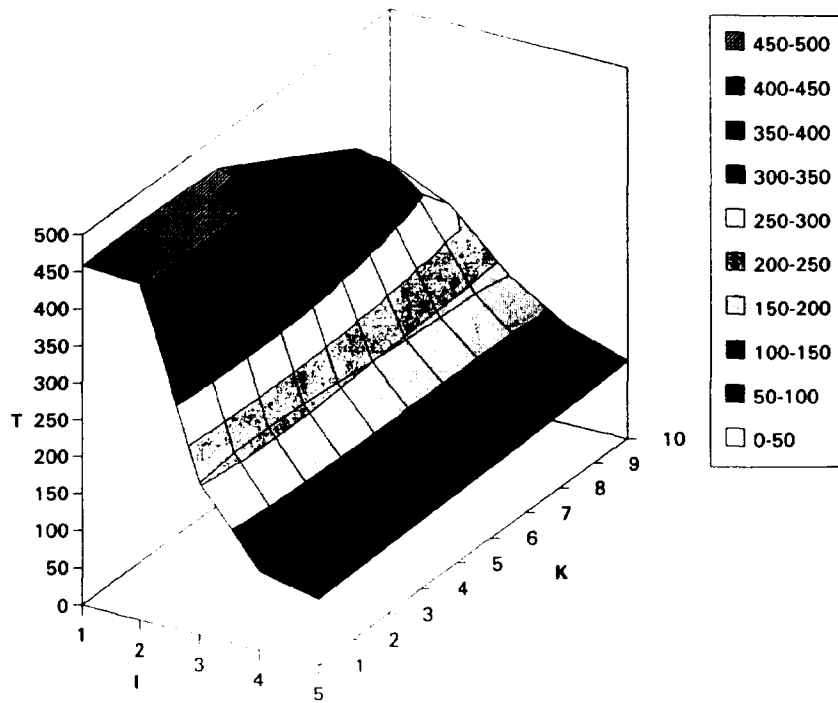Alternate representation of dual-permeability grid. Arrows denote connections between gridcells.

Figure 4.   Temperature in fractures at five years for two-dimensional example.
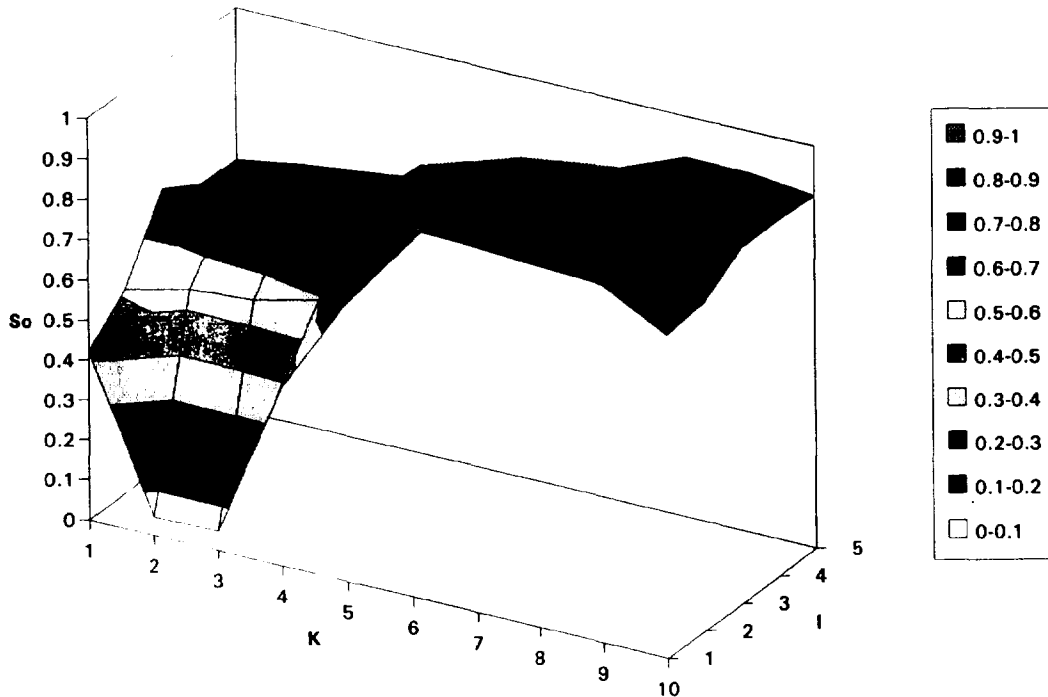

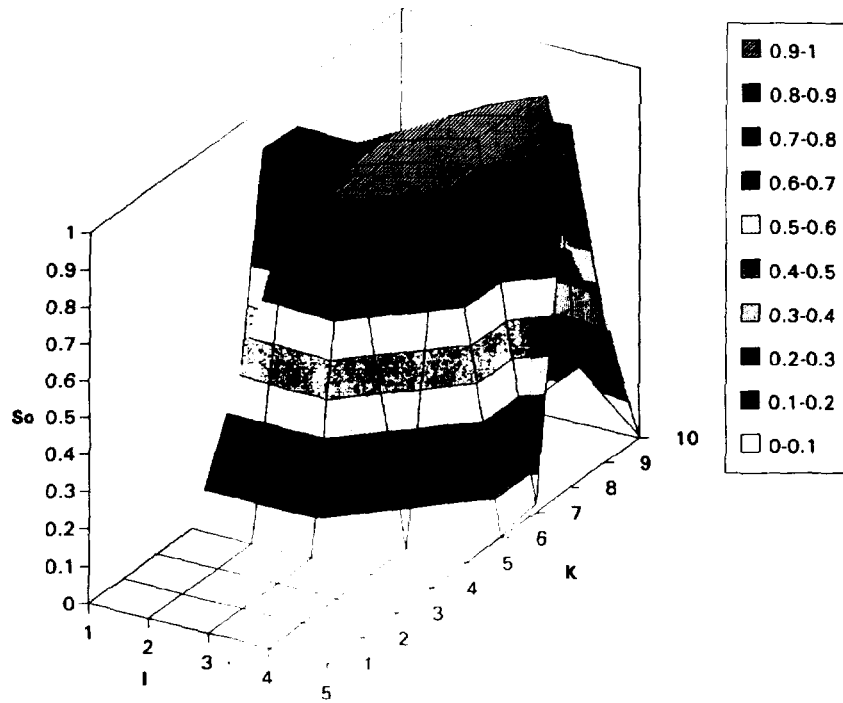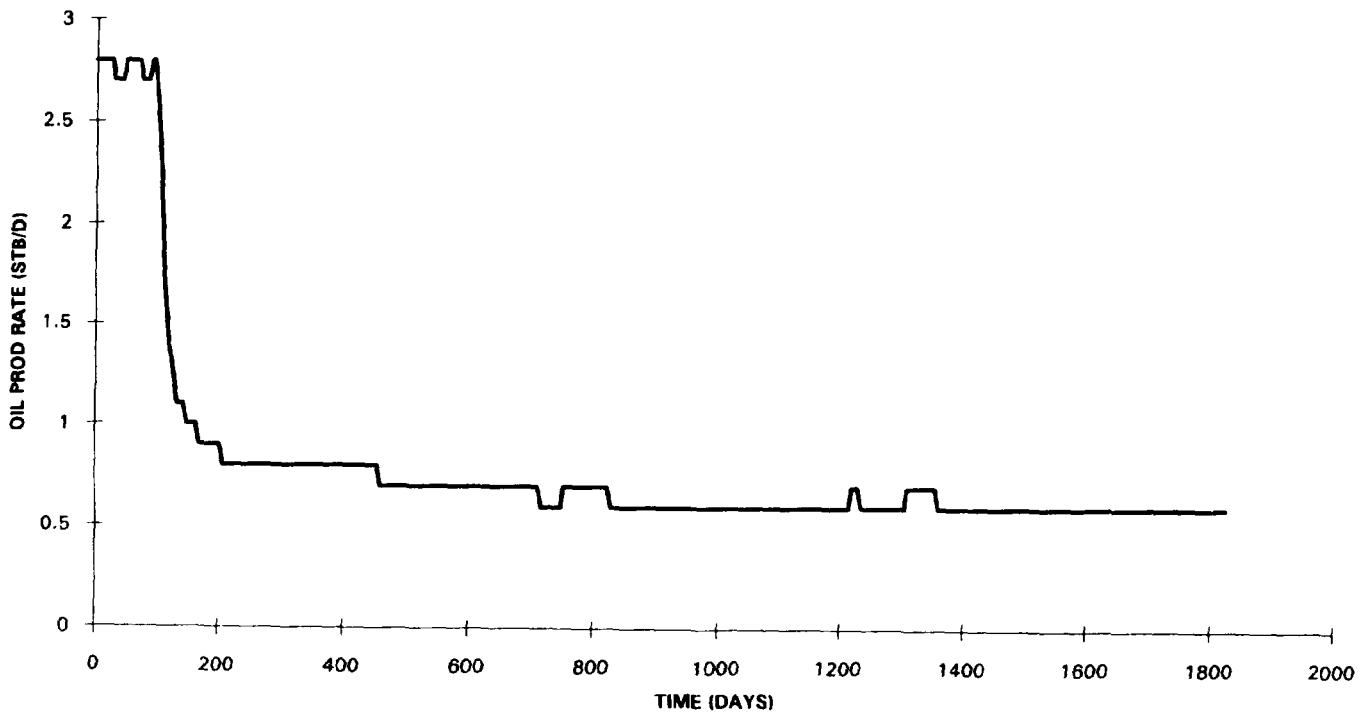**Figure 5a.   Oil saturation in matrix at five years for two-dimensional example.**

Figure 5b. Oil saturation in fractures at five years for two-dimensional example.

Figure 6. Oil production rate versus time for two-dimensional example.

227
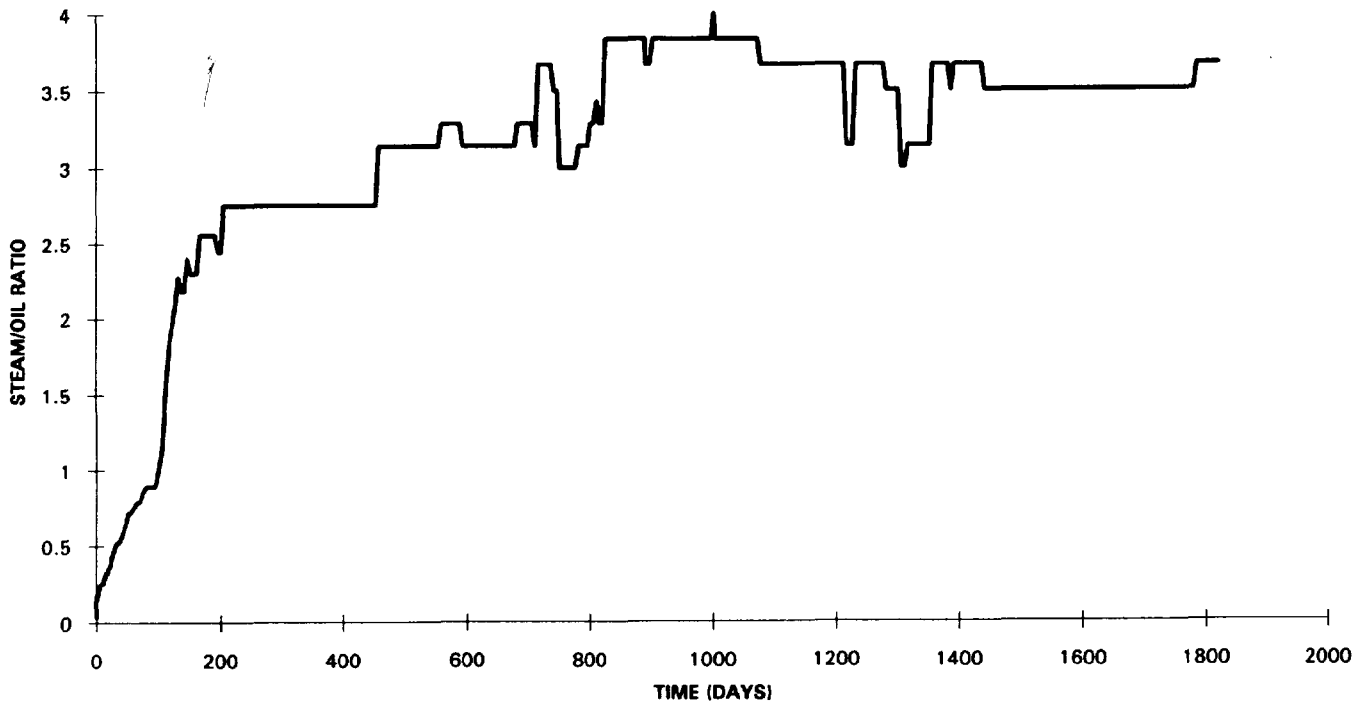
Figure 7.   Steam/oil ratio versus time for two-dimensional example.
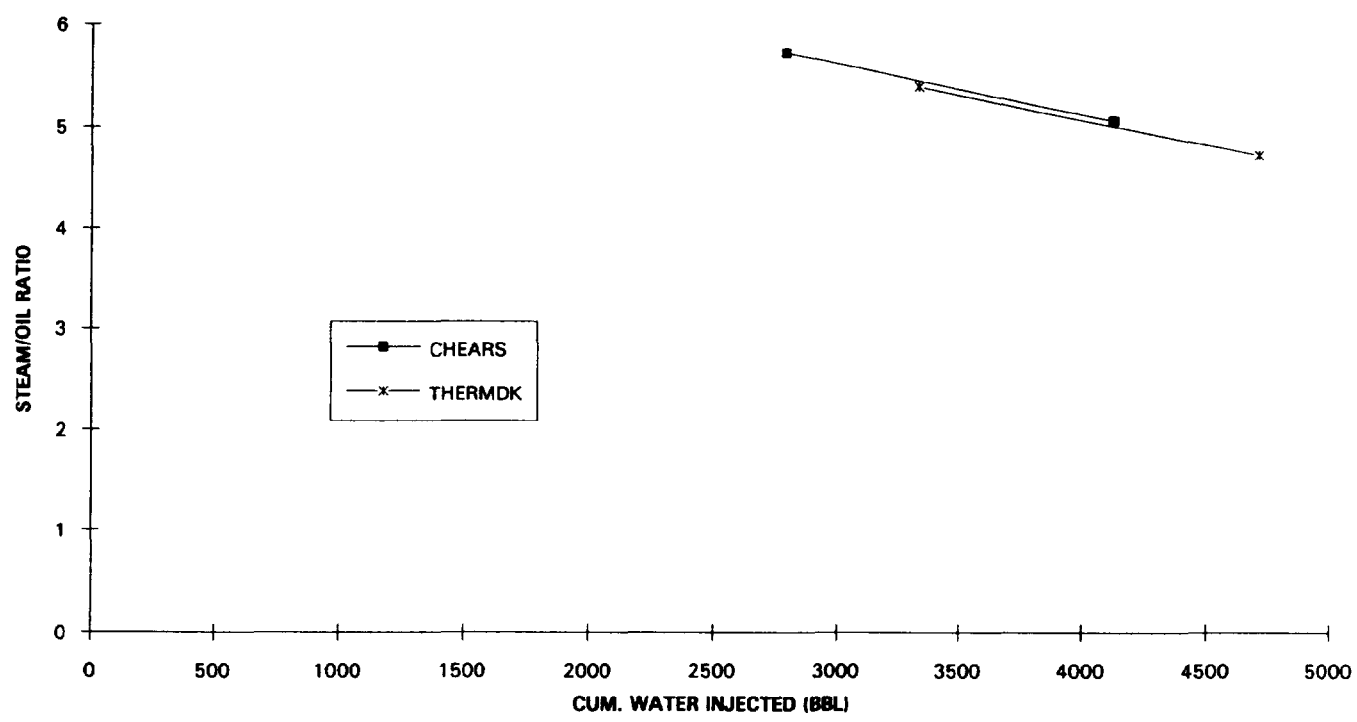
Figure 8.   Comparison of CHEARS and THERMDK steam/oil ratio after five years of steam injection.

228
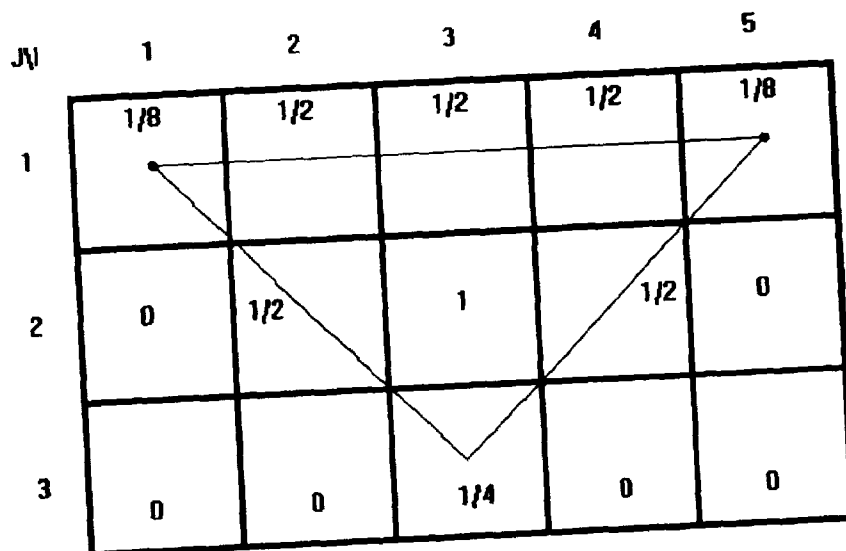
Figure 9. Cross section (xy) of grid for three-dimensional example showing outline of eighth of ten acre pattern. Numbers in gridcells indicate geometry correction factors.
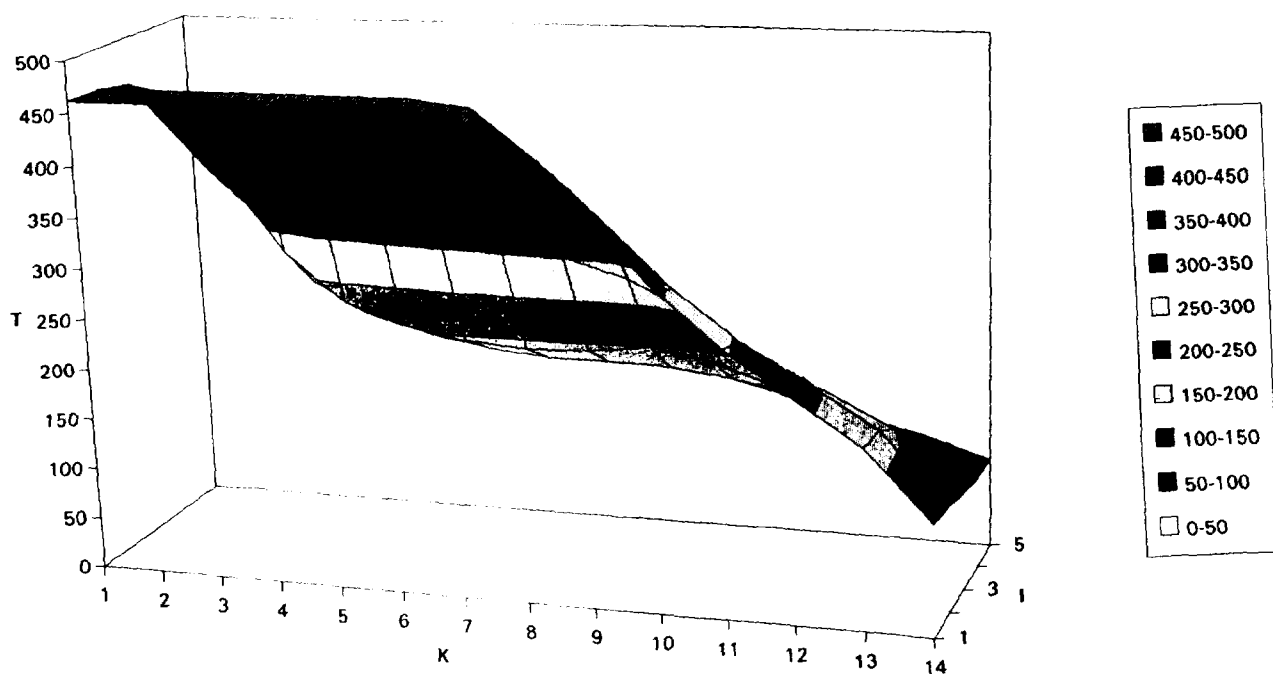
Figure 10a. Fracture temperature in vertical plane containing both wells at 3 ½ years.
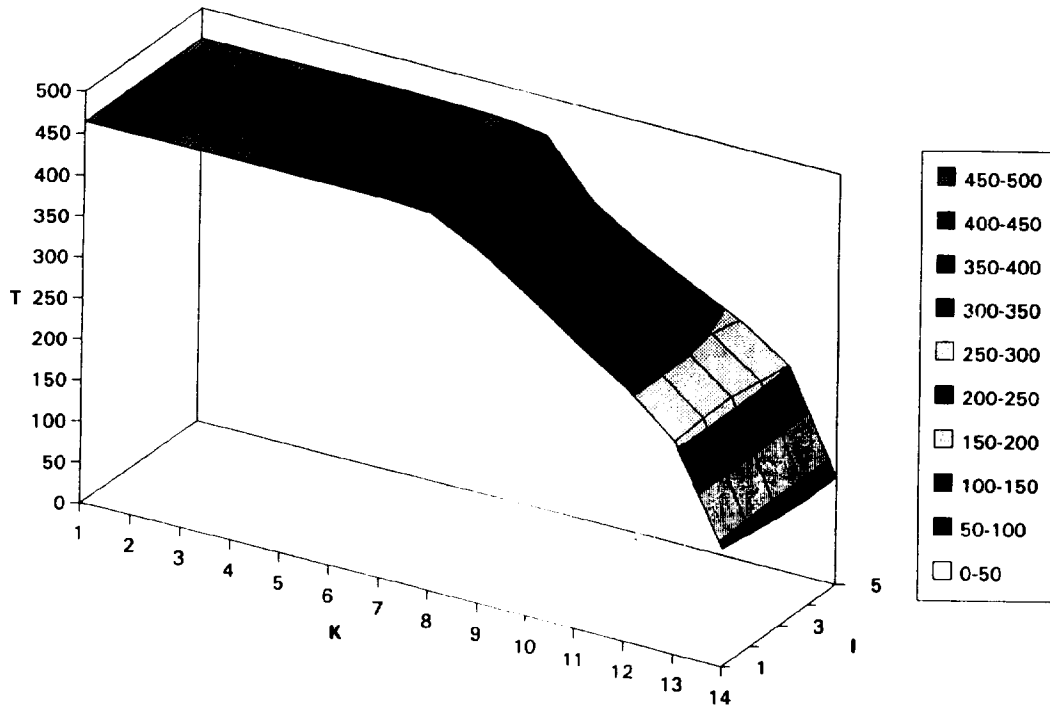
Figure 10b. Fracture temperature in vertical plane containing both wells at 7 years.
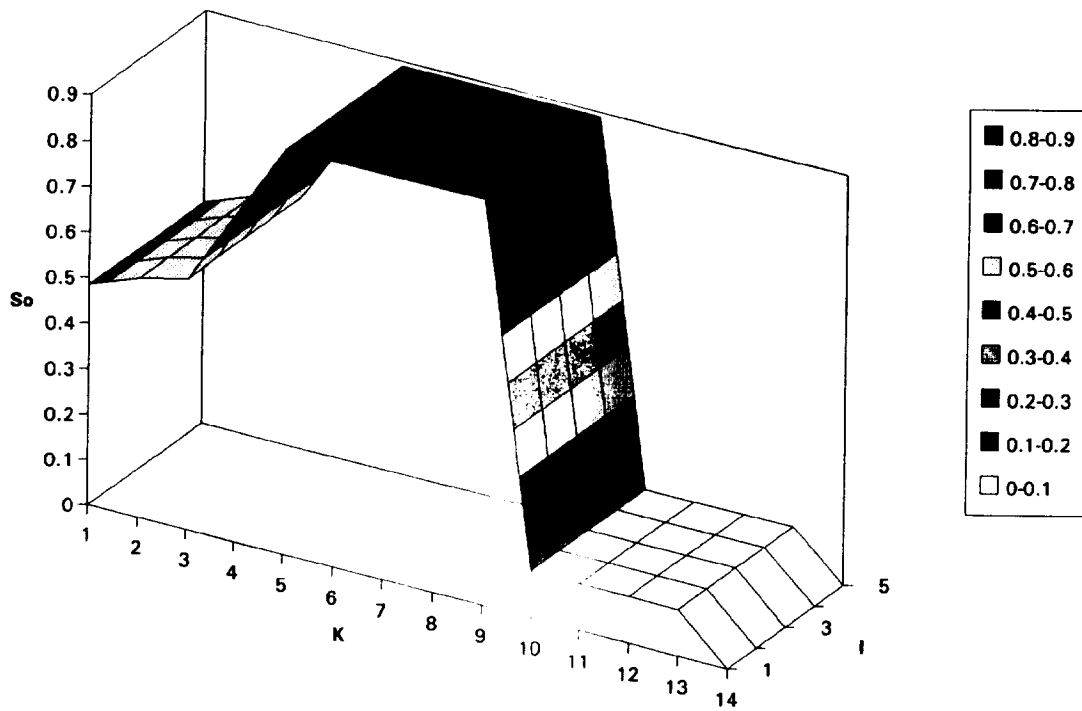
Figure 11a. Initial matrix oil saturation in vertical plane containing both wells.
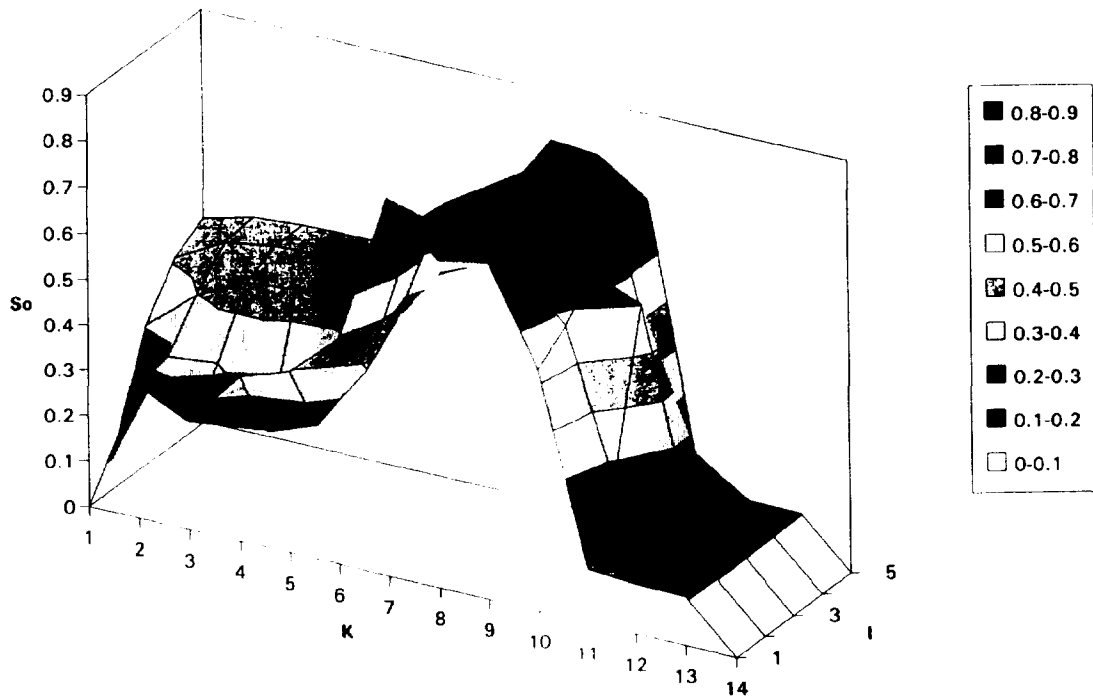
Figure 11b. Matrix oil saturation at 3 ½ years in vertical plane containing both wells.
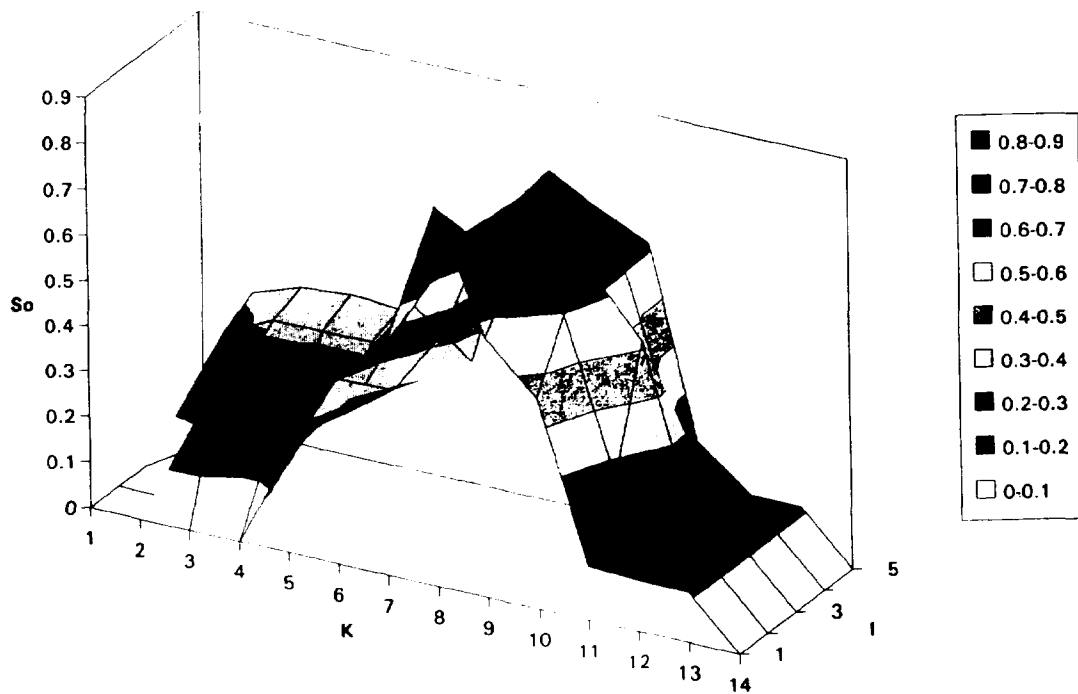

Figure 11c. Matrix oil saturation at 7 years in vertical plane containing both wells.
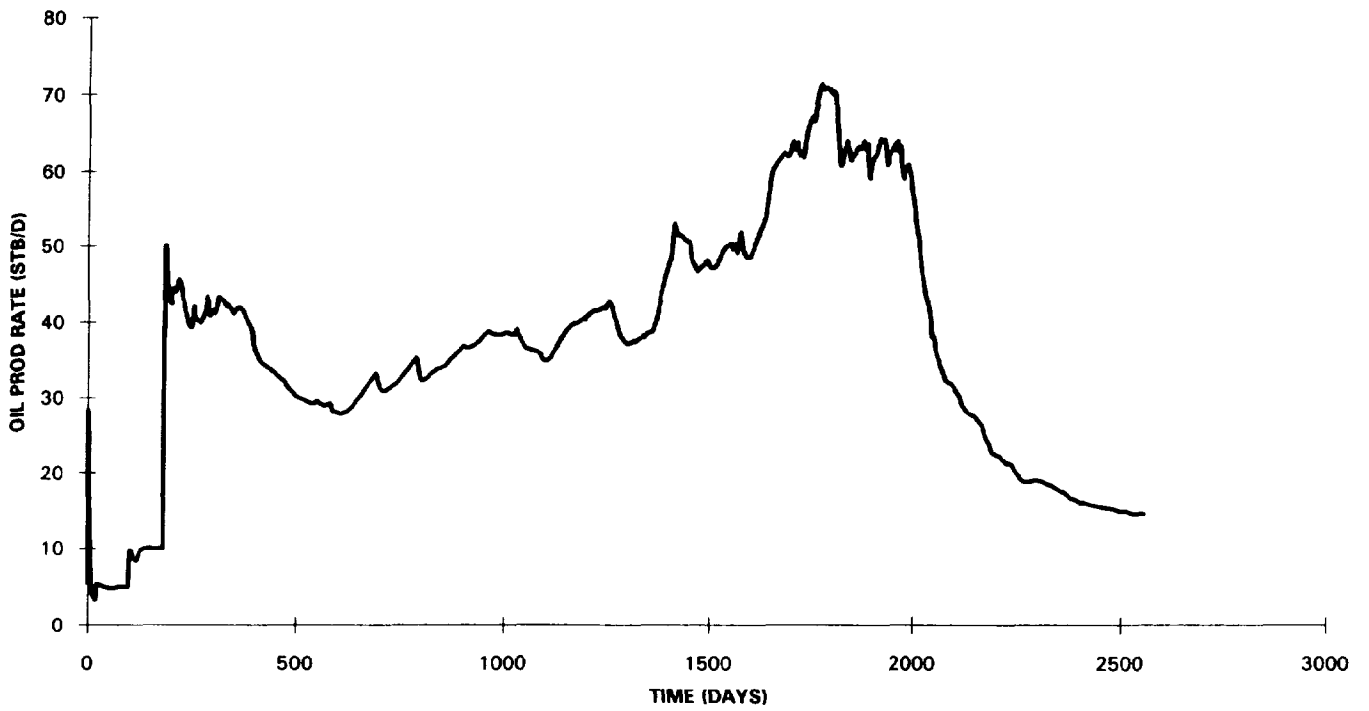
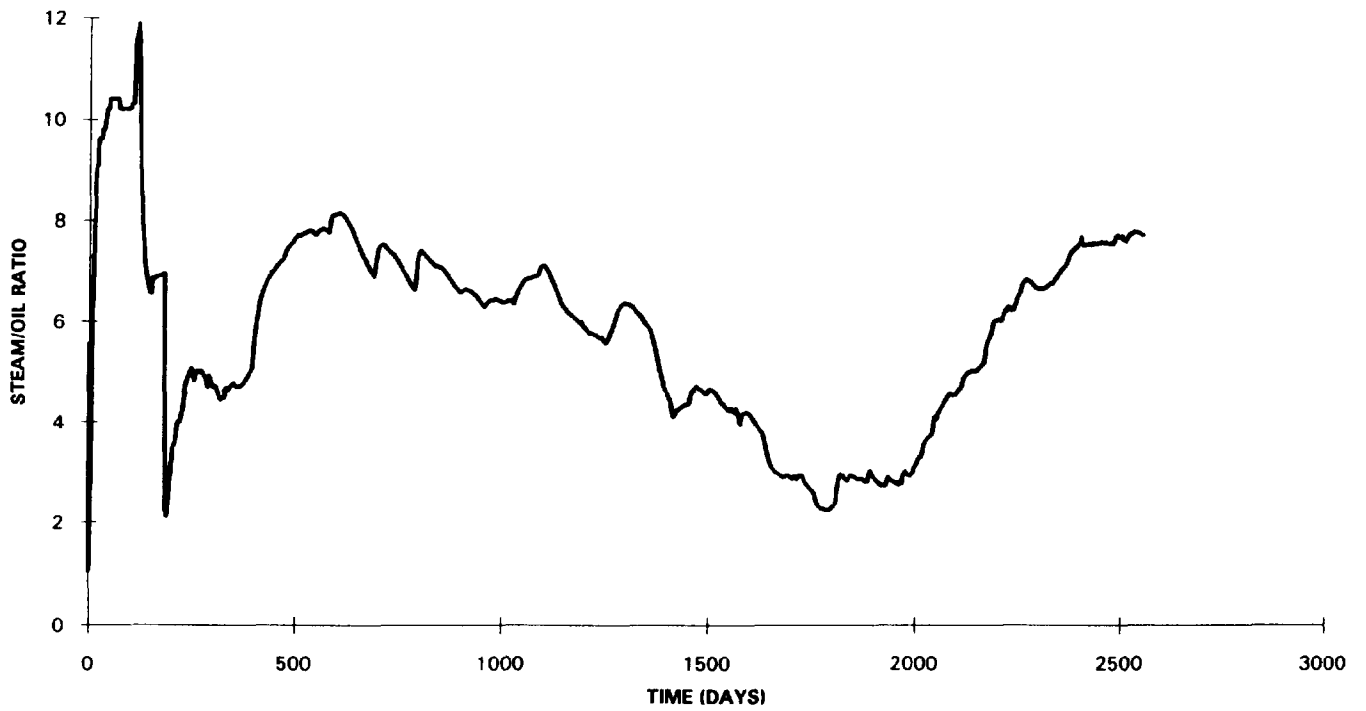Figure 12. Oil production rate versus time for three-dimensional example.

Figure 13. Steam/oil ratio versus time for three-dimensional example.

232